



## Effect of Temperature on the Crevice Corrosion of Nickel Alloys Containing Chromium and Molybdenum

E. C. Hornus,<sup>a</sup> C. M. Giordano,<sup>a</sup> M. A. Rodríguez,<sup>a,b,\*</sup> R. M. Carranza,<sup>a</sup> and R. B. Rebak<sup>c,\*</sup>

<sup>a</sup>Gerencia Materiales, Comisión Nacional de Energía Atómica, Instituto Sabato, UNSAM / CNEA, San Martín,  
B1650KNA Buenos Aires, Argentina

<sup>b</sup>Consejo Nacional de Investigaciones Científicas y Técnicas, Buenos Aires, Argentina

<sup>c</sup>GE Global Research, Schenectady, New York 12309, USA

Chloride-induced crevice corrosion of alloys 625, C-22, C-22HS and HYBRID-BC1 was studied at different temperatures. Crevice corrosion occurred tens of degrees below the reported critical crevice temperatures obtained through standard immersion tests. Concentrated calcium and sodium chloride solutions showed the same aggressiveness regarding crevice corrosion behavior of alloys C-22 and HYBRID-BC1. The crevice corrosion repassivation potential decreased as the temperature and chloride concentration increased. For alloys 625 and C-22, the repassivation potential reached a minimum limiting value which was coincident with the corrosion potential in the crevice-like solution. For alloys C-22HS and HYBRID-BC1, these conditions are expected to be reached above the tested temperatures. The high dependence of the repassivation potential on chloride concentration was attributed to the ohmic potential drop caused by passivating species at the alloy/solution interface. A temperature dependence of 4–9 mV/K was observed for the repassivation potential in dilute chloride solutions while it decreased to 2–3 mV/K in concentrated chloride solutions. In the context of the localized acidification model, the corrosion potential in the crevice-like solution did not depend on the temperature while the anodic polarization to maintain the crevice acidity and the ohmic potential drop decreased linearly as temperature increased.

© 2014 The Electrochemical Society. [DOI: [10.1149/2.0431503jes](https://doi.org/10.1149/2.0431503jes)] All rights reserved.

Manuscript submitted October 7, 2014; revised manuscript received December 12, 2014. Published December 23, 2014.

Nickel alloys containing chromium and molybdenum find several industrial applications in conditions where a high resistance to localized corrosion is needed.<sup>1</sup> These alloys may suffer localized corrosion in the forms of pitting and crevice corrosion when exposed to hot chloride solutions.<sup>2</sup> Temperature and chloride concentration are among the key parameters affecting the susceptibility of the alloys to localized attack.<sup>1–3</sup> Crevice and pitting corrosion are essentially the same phenomena from an electrochemical point of view.<sup>4</sup> Pitting and crevice corrosion show the same dependence with potential and chloride concentration; and there are critical pitting and crevice corrosion temperatures (CPT and CCT, respectively) below which pitting and crevice corrosion do not occur.<sup>2</sup> However, crevice corrosion is observed in occluded surfaces (such as cracks and crevices) while pitting corrosion occurs in surfaces openly exposed to the corrosive environment. Crevice corrosion is of particular concern for nickel alloys containing large amounts of chromium and molybdenum since they are practically immune to pitting corrosion.<sup>3,5</sup>

The PRE (Pitting Resistance Equivalent) is frequently used as an indicative measure of the alloys resistance to localized corrosion. PRE is defined in Equation 1 as a function of the weight percentages of the alloying elements Cr, Mo and W.<sup>2</sup> The applicability of PRE for nickel alloys containing chromium and molybdenum has been discussed recently.<sup>6,7</sup>

$$\text{PRE} = \% \text{Cr} + 3.3 (\% \text{Mo} + 0.5\% \text{W}) \quad [1]$$

Above the CCT, the crevice corrosion resistance of an alloy in a given environmental condition is usually measured by its repassivation potential ( $E_{\text{R,REV}}$ ).<sup>8,9</sup>  $E_{\text{R,REV}}$  may be measured as a function of temperature and chloride concentration leading to accurate ranges of environmental conditions for crevice corrosion occurrence. This is an advantage when compared to the use of critical temperatures, such as CCT, which do not provide precise information of the potential ranges for crevice corrosion occurrence. Moreover,  $E_{\text{R,REV}}$  is more conservative and reproducible than the crevice corrosion initiation potential ( $E_{\text{CREV}}$ ).<sup>2</sup> The higher the  $E_{\text{R,REV}}$  the higher the crevice corrosion resistance of the alloy. This parameter may be obtained by a variety of testing methods.<sup>10</sup> In service conditions, crevice corrosion only occurs if the corrosion potential of the alloy ( $E_{\text{CORR}}$ ) exceeds  $E_{\text{R,REV}}$ . However, this is a necessary but not a sufficient condition. Crevice corrosion may not occur even though  $E_{\text{CORR}} > E_{\text{R,REV}}$  due

to the lack of a demanding crevice. A demanding crevice is a tight crevice formed with a non-metallic and non-porous crevice former. In-service crevices may be less demanding than those used for crevice corrosion testing since the latter are specifically developed for obtaining reproducible and conservative results.<sup>11–13</sup> Crevice corrosion in service also needs at least one cathodic reaction to support the anodic process. Cathodic limitations may arise from the inhibition of cathodic reactions occurring on the passivated alloy.<sup>14,15</sup> In general, the use of  $E_{\text{R,REV}}$  as a critical parameter for comparing different alloys relies on the assumption that there are no cathodic limitations and a tight crevice is formed on the alloy surface. In spite of these limitations,  $E_{\text{R,REV}}$  is a useful parameter to rank the crevice corrosion resistance of engineering alloys, the effects of inhibitors, heat treatments, etc. Moreover,  $E_{\text{R,REV}}$  is one of the commonly selected parameters to study the anodic kinetics of localized corrosion.<sup>2,6,8–13,16–20</sup>  $E_{\text{R,REV}}$  is statistically distributed and its dispersion generally increases as the testing conditions become less aggressive. Some authors calculate the crevice survival probabilities and crevice generation rates from  $E_{\text{R,REV}}$  values by applying a stochastic theory.<sup>18,19</sup>

Several researchers have applied the localized acidification model, developed by Galvele<sup>21</sup> and later modified by Newman et al.,<sup>22–25</sup> to interpret the crevice corrosion of nickel alloys containing chromium and molybdenum.<sup>5,6,12,16,26</sup> This model indicates that the crevice corrosion repassivation potential is the sum of three contributions, as stated in Equation 2.<sup>21</sup>  $E_{\text{CORR}}^*$  is the corrosion potential of the alloy in the local acidic solution (in this case, the crevice-like solution);  $\eta$  is the anodic polarization needed to attain  $(x_i)_{\text{CRIT}}$ , which is the critical value of the product of the diffusion path ( $x$ ) and the current density ( $i$ ) to sustain crevice corrosion; and  $\Delta\Phi$  is the ohmic potential drop within the crevice.<sup>21</sup>

$$E_{\text{R,REV}} = E_{\text{CORR}}^* + \eta + \Delta\Phi \quad [2]$$

This model has been previously applied to the crevice corrosion of nickel alloys containing chromium and molybdenum leading to a better understanding of this system. For instance (1) Rodríguez et al.<sup>5</sup> explained the absence of pitting corrosion on alloy C-22 at any applied potential, (2) Rincón et al.<sup>12</sup> rationalized different effects of the localized corrosion propagation on the diffusion path in crevice and pitting corrosion, (3) Zadorozne et al.<sup>6</sup> obtained insights on the crevice corrosion kinetics of alloys C-22, C-22HS and HYBRID-BC1, and (4) Bocher et al.<sup>26</sup> predicted critical potentials for the crevice corrosion initiation of alloys 625 and C-22.

\*Electrochemical Society Active Member.

<sup>a</sup>E-mail: [maalrod@cnea.gov.ar](mailto:maalrod@cnea.gov.ar); [martinrz@gmail.com](mailto:martinrz@gmail.com)

The localized acidification model may be used to predict  $E_{R,CREV}$  by measuring or calculating the three terms of Equation 2 ( $E_{CORR}^*$ ,  $\eta$  and  $\Delta\Phi$ ).  $E_{CORR}^*$  may be determined in HCl solutions simulating the acidic conditions within active crevices.  $\eta$  may be estimated from polarization curves in the crevice-like solution. However, there is some uncertainty regarding the current density needed to reach  $(x_i)_{CRIT}$  since both  $x$  and  $(x_i)_{CRIT}$  are unknown. The criterion of stable localized corrosion for  $(x_i)_{CRIT} > 0.01 \text{ A/cm}$  developed for pitting of stainless steels is not appropriate for the crevice corrosion of nickel alloys.<sup>6</sup> The calculation of  $\Delta\Phi$  is also difficult since an effective resistivity of the solution should be assumed incorporating the effects of tortuosity, debris, and corrosion products.<sup>26</sup>

Temperature has an important effect on the crevice corrosion resistance of stainless steels and nickel based alloys. Published research is focused on the determination of crevice corrosion critical potentials as a function of temperature,<sup>18,20,27</sup> crevice corrosion critical temperatures<sup>27,28</sup> or both types of parameters<sup>7,17</sup> (critical potentials and temperatures). Jakobsen and Maahn<sup>27</sup> indicated that crevice corrosion breakdown potentials for 316 stainless steel decrease with increasing temperatures within a transition temperature interval. Evans et al.<sup>20</sup> studied the crevice corrosion of alloy C-22 under different metallurgical conditions in 5 mol/L  $\text{CaCl}_2$  in a wide temperature range. They reported that  $E_{R,CREV}$  decreases steeply as the temperature increases in the temperature range from 30°C to 60°C, while it decreases more gradually in the range from 60°C to 120°C. Results from literature suggest that crevice corrosion resistance varies significantly in a certain temperature range while it remains almost constant for high temperatures. The temperature dependence of critical potentials varies among alloys.<sup>7,18</sup>

Valen and Gartland<sup>28</sup> studied the repassivation temperature of UNS S31254 and S32750 stainless steels. They performed cyclic temperature scans on creviced specimens and reported large current hysteresis. These authors concluded that once the crevice corrosion initiates at a given temperature, it may propagate at lower temperatures. This finding suggests the existence of a crevice protection temperature ( $T_{PROT}$ ) which is below CCT. Abd El Meguid and Abd El Latif<sup>29</sup> reported CCT = 55°C and  $T_{PROT} = 52^\circ\text{C}$  for 254 SMO stainless steel in 4% NaCl. Mishra and Frankel<sup>17</sup> reported a repassivation temperature ( $T_{R,CREV}$ ) of 65°C and suggested  $T_{PROT} = 60^\circ\text{C}$  for alloy C-22. According to these authors,  $T_{R,CREV}$  is the temperature at which a growing crevice corrosion repassivates, whereas  $T_{PROT}$  is the temperature below which crevice corrosion will not initiate.<sup>17</sup> Reported differences among CCT,  $T_{R,CREV}$  and  $T_{PROT}$  are small (3 to 5°C).<sup>17,29</sup> Mishra and Shoesmith<sup>7</sup> reported  $T_{PROT}$  is 25°C for alloy 625,  $T_{PROT} = 30^\circ\text{C}$  for alloy C-4,  $T_{PROT} = 40^\circ\text{C}$  for alloy C-276,  $T_{PROT} = 55^\circ\text{C}$  for alloys 59, C-22 and C-2000, and  $T_{PROT} = 75^\circ\text{C}$  for alloy 686. The CCT reported in the literature for Ni-Cr-Mo alloys varies between 40°C and 125°C.<sup>30</sup>

The effectiveness of crevice corrosion inhibitors also varies with temperature. Ilebvarie<sup>31</sup> indicated that sulfate is a less effective crevice corrosion inhibitor for alloy C-22 as temperature increases. On the contrary, molybdate is reported to increase its inhibiting effect at high temperatures.<sup>32</sup>

The objective of the present study is to assess the effect of temperature on the crevice corrosion resistance of nickel alloys containing chromium and molybdenum in chloride solutions. This assessment includes the determination of critical temperatures below which crevice corrosion does not occur and a comprehensive study of  $E_{R,CREV}$  as a function of temperature and chloride concentration for alloys 625, C-22, C-22HS and HYBRID-BC1. These alloys were selected to

cover a wide range of chemical compositions within the Ni-Cr-Mo alloy family. The cation effect on crevice corrosion was evaluated in equal chloride concentrations of  $\text{NaCl}$  and  $\text{CaCl}_2$ . The localized acidification model was applied for determining the relative contributions of  $E_{CORR}^*$ ,  $\eta$  and  $\Delta\Phi$  to  $E_{R,CREV}$ .

## Experimental

The specimens were prepared from wrought mill annealed (MA) plate stock. The chemical compositions of the tested alloys along with their PRE values are listed in Table I. Prism Crevice Assembly (PCA) specimens were used (ASTM G 192).<sup>33</sup> These specimens contain 24 artificially creviced spots formed by two ceramic washers (crevice formers) wrapped with a 70  $\mu\text{m}$ -thick polytetrafluoroethylene (PTFE) tape. The applied torque to the crevice formers was 5 N·m. The tested surface area was approximately 14  $\text{cm}^2$ . The specimens had a grinding of abrasive paper number 600 and were degreased in acetone and washed in distilled water within the hour prior to testing.

All the electrochemical tests were conducted in a one-liter, three-electrode vessel. Nitrogen ( $\text{N}_2$ ) was purged through the solution 1 hour prior to testing and it was continued throughout the entire test. A water-cooled condenser combined with a water trap was used to avoid evaporation of the solution and to prevent the ingress of air (oxygen). The temperature of the solution was controlled by immersing the cell in a liquid bath, which was kept at a constant temperature. All the tests were performed at ambient pressure. The reference electrode was a saturated calomel electrode (SCE), which has a potential of 0.242 V more positive than the standard hydrogen electrode (SHE). The reference electrode was connected to the solution through a water-cooled Luggin probe and it was kept at room temperature. The electrode potentials were not corrected for the thermal liquid junction potential since it was assumed to be on the order of a few mV. The counter electrode consisted in a flag of platinum foil (total area 50  $\text{cm}^2$ ) spot-welded to a platinum wire. All the potentials in this paper are reported in the SCE scale.

The crevice corrosion repassivation potential was determined by the potentiodynamic-galvanostatic-potentiodynamic (PD-GS-PD) method.<sup>6,10,12,17</sup> This is a modification of the Tsujikawa-Hisamatsu electrochemical method (ASTM G 192)<sup>33</sup> which has led to the most conservative results among crevice corrosion testing methods.<sup>10,12</sup> The PD-GS-PD method consists of three stages: (1) a potentiodynamic polarization (at a scan rate of 0.167 mV/s) in the anodic direction up to reaching an anodic current of 30 or 300  $\mu\text{A}$ , (2) the application of a constant anodic current of  $I_{GS} = 30 \mu\text{A}$  or  $I_{GS} = 300 \mu\text{A}$  (approximately  $i_{GS} = 2 \mu\text{A}/\text{cm}^2$  or  $i_{GS} = 20 \mu\text{A}/\text{cm}^2$ ) for 2 hours, and (3) a potentiodynamic polarization (at 0.167 mV/s) in the cathodic direction, from the potential at the end of stage 2 until reaching alloy repassivation. At least three PD-GS-PD tests were performed for each alloy in each testing condition. Before each PD-GS-PD test, the open circuit potential was measured for 15 minutes and afterwards a cathodic current of 50  $\mu\text{A}$  was applied for 5 minutes (pre-treatment). A  $I_{GS} = 300 \mu\text{A}$  was set in the tests performed on alloy HYBRID-BC1 at temperatures below 100°C, while a  $I_{GS} = 30 \mu\text{A}$  was used in tests at 100°C, 110°C and 117°C. For alloys 625, C-22 and C-22HS, a  $I_{GS} = 300 \mu\text{A}$  was set in tests below 70°C, while a  $I_{GS} = 30 \mu\text{A}$  was used in tests at temperatures in the range from 70°C to 117°C. The value of  $I_{GS}$  was increased for the low temperature range in order to decrease the incubation time for crevice corrosion initiation. This

**Table I.** Chemical composition of the tested alloys in weight percent.

Alloy	Ni	Cr	Mo	W	Fe	Co	Si	Mn	C	V	Al	B	Nb+Ta	PRE
625	62	21	9	0	5	1	0.5	0.5	0.1	0	0.4	0	3.7	51
C-22	56	22	13	3	3	2.5	0.08	0.5	0.01	0.35	0	0	0	70
C-22HS	61	21	17	1	2	1	0.08	0.8	0.01	0	0.5	0.006	0	79
HYBRID-BC1	62	13	22	0	2	0	0.08	0.25	0.01	0	0.5	0	0	88

change is not expected to affect significantly the obtained value for  $E_{R,CREV}$ .<sup>10,17</sup>

The testing solutions were 0.1 mol/L NaCl, 1 mol/L NaCl and 5 mol/L CaCl<sub>2</sub>. That is, the chloride concentration ( $[Cl^-]$ ) was varied from 0.1 to 10 mol/L. The tests were performed in the temperature range from 20°C to 90°C in 0.1 and 1 mol/L NaCl solutions, and in the range from 20°C to 117°C in 5 mol/L CaCl<sub>2</sub> solutions. CaCl<sub>2</sub> was used to prepare the  $[Cl^-] = 10$  mol/L solution due to its higher solubility. This solution has a high ionic strength and the activity coefficient of chloride may differ from unity. Rodil and Vera measured the activity coefficients of chloride in CaCl<sub>2</sub> solutions at room temperature.<sup>34</sup> However, these authors used CaCl<sub>2</sub> concentrations up to 3 mol CaCl<sub>2</sub>/kg H<sub>2</sub>O while 5 mol/L CaCl<sub>2</sub> corresponds to 5.9 mol CaCl<sub>2</sub>/kg H<sub>2</sub>O. Extrapolation of Rodil and Vera's results leads to an activity coefficient of chloride between 0.5 and 0.7 in 5 mol/L CaCl<sub>2</sub> solution at room temperature. However, extrapolation of data from the hydration model of Bates et al. indicates an activity coefficient of chloride of approximately 1.3 in the same conditions.<sup>34,35</sup> Activity coefficients of chloride in 5 mol/L CaCl<sub>2</sub> are not available for the tested temperature range. Therefore, chloride concentration was used instead of activity for the 5 mol/L CaCl<sub>2</sub> solution.

Another set of tests was performed in 4 mol/L NaCl and 2 mol/L CaCl<sub>2</sub> at 60, 70 and 80°C aiming to assess the effect of the electrolyte salt cations on crevice corrosion. All the specimens were examined after testing with a light optical microscope (LOM) and some of them were observed in the scanning electron microscope (SEM).

The corrosion potential of the tested alloys was measured for 2 hours in deaerated HCl solutions, at temperatures ranging from 30°C to 100°C. Testing solutions included 1 mol/L and 3 mol/L HCl aiming to simulate the conditions in active crevices. Non-creviced prismatic specimens of the tested alloys were used. Surface finishing of specimens and experimental setup were identical to those previously described for the PD-GS-PD tests.<sup>12</sup> Degaeration was limited to 30 minutes prior to each experiment and it was continued throughout the entire test. Immersion time was limited to 2 hours since N<sub>2</sub> bubbling used to displace O<sub>2</sub> may also displace gaseous HCl. This may lead to the dilution of the acidic solution.  $E_{CORR}$  stabilized below 1 mV/hour within the 2 hours of immersion in most of cases.

## Results

**Crevice corrosion tests.**— Figure 1 shows PD-GS-PD tests performed on the four nickel alloys in 5 mol/L CaCl<sub>2</sub>, at 110°C. All the tests showed a cathodic branch followed by a passive range with current densities from 0.5 to 1  $\mu A/cm^2$ , and then a current increase due to the breakdown of passivity. The forward potential scan (stage 1) for alloy 625 started 0.1 V above those of alloys C-22, C-22HS and

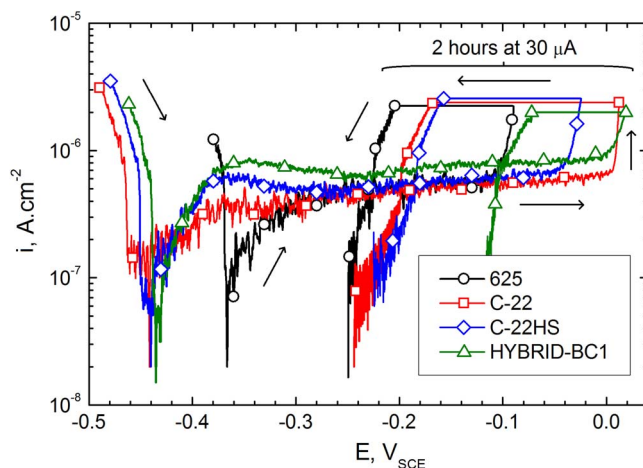


**Figure 1.** PD-GS-PD tests (stages 1, 2 and 3) performed on nickel alloys in 5 mol/L CaCl<sub>2</sub>, at 110°C.

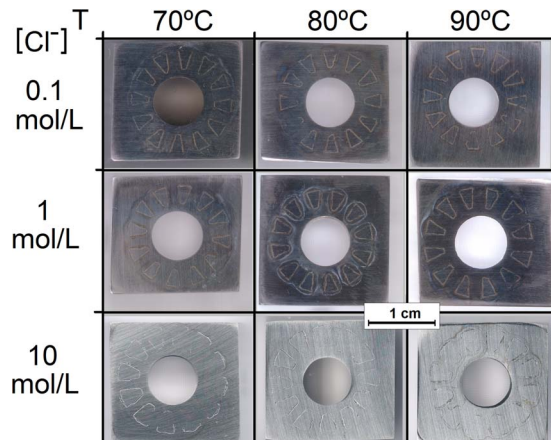


**Figure 2.** Images of alloy HYBRID-BC1 specimens after PD-GS-PD tests performed in chloride solutions at different temperatures.

HYBRID-BC1. This feature was observed in several tests performed in different alloys and it was attributed to variability in the specimen preparation which did not affect the determination of the repassivation potentials. The passive current density of alloy HYBRID-BC1 was higher than those of alloys 625, C-22 and C-22HS in all the tested conditions. This was a consequence of the lower Cr and higher Mo content of alloy HYBRID-BC1 in comparison to the other tested alloys.<sup>6</sup> During the galvanostatic step (stage 2) the potential dropped due to the crevice corrosion propagation. This is observed as a constant current density of approximately 2  $\mu A/cm^2$  within a potential range in Figure 1. In stage 3, the current density decreased sharply at the beginning of the reverse potential scan (Fig. 1). The  $E_{R,CREV}$  for each test was selected as the cross-over potential determined at the intersection of the forward (stage 1) and reverse (stage 3) scans.

Figure 2 shows specimens of alloy HYBRID-BC1 after testing in solutions with different chloride concentrations at 70, 80 and 90°C. The specimens tested in 0.1 and 1 mol/L NaCl solutions had a similar appearance showing corrosion products on the alloy surface below the crevice former teeth, while the corrosion products were practically absent in those specimens tested in 5 mol/L CaCl<sub>2</sub>. Microscopic observation of the four tested alloys indicated that the area of crevice corrosion attack moved outwards (to the crevice mouth) as the chloride concentration increased. Figure 3 shows SEM images of crevice corroded alloy C-22 after testing in solutions with different chloride concentrations, at temperatures from 40°C to 90°C. As observed for alloy HYBRID-BC1 (Fig. 2), alloy C-22 specimens tested in 0.1 and 1 mol/L NaCl solutions showed abundant corrosion products while

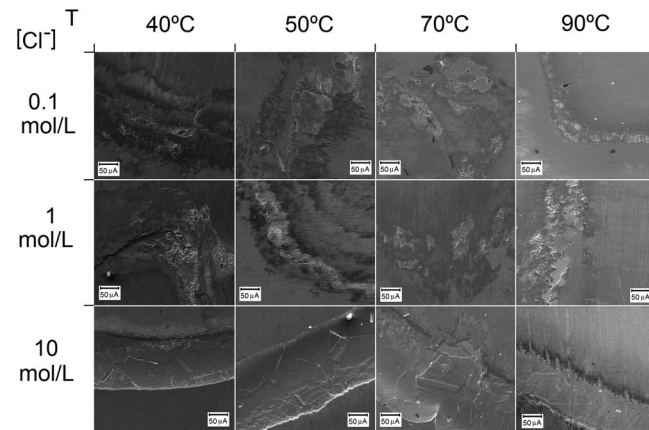


**Figure 3.** SEM images of alloy C-22 specimens after PD-GS-PD tests performed in chloride solutions at different temperatures.

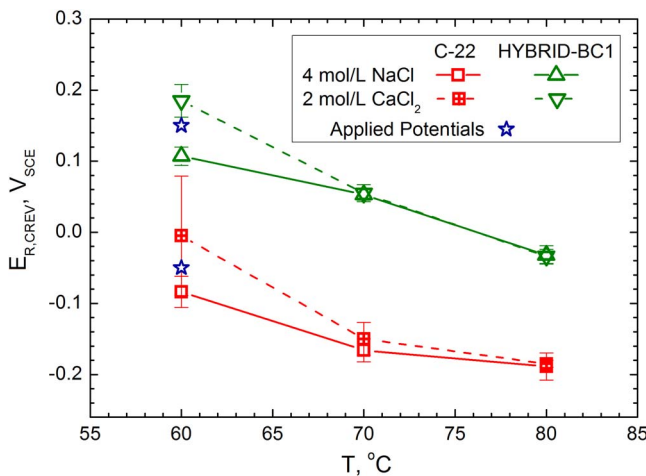


**Figure 4.**  $E_{R,CREV}$  as a function of temperature for alloys C-22 and HYBRID-BC1 in 4 mol/L NaCl and 2 mol/L CaCl<sub>2</sub> solutions.

specimens tested in 5 mol/L CaCl<sub>2</sub> did not show significant corrosion products. All the tested alloys showed the same localized attack morphology: discernible alloy grains in the attacked areas (especially in 5 mol/L CaCl<sub>2</sub> solutions) and preferential attack at triple points, as reported elsewhere.<sup>6,8,12,36</sup> The increase of [Cl<sup>-</sup>] from 1 to 10 mol/L led to a lesser amount of corrosion products for all the tested alloys. Temperature did not show an important effect on the localized attack morphology, in the tested conditions.

**Effect of cations.**— Previous works shows that  $E_{R,CREV}$  for alloy C-22 in 1 mol/L chloride solutions at 90°C is not affected by the cations Na<sup>+</sup>, K<sup>+</sup>, Ca<sup>2+</sup> and Mg<sup>2+</sup>.<sup>37</sup> However, increasing chloride concentration from 4 mol/L (as NaCl) to 10 mol/L (as CaCl<sub>2</sub>) produced a slight increase of  $E_{R,CREV}$  for alloys C-22 and C-22HS.<sup>6,12</sup> In this work, we studied the effect of cations Na<sup>+</sup> and Ca<sup>2+</sup> on  $E_{R,CREV}$  since the localized attack morphology significantly changed when [Cl<sup>-</sup>] varied from 1 to 10 mol/L, but at the same time the cation identity changed (Na<sup>+</sup> to Ca<sup>2+</sup>). The cation effect was assessed on alloys C-22 and HYBRID-BC1.

Figure 4 shows  $E_{R,CREV}$  as a function of temperature for alloys C-22 and HYBRID-BC1 in 4 mol/L NaCl and 2 mol/L CaCl<sub>2</sub>. The points are average values from three tests and the error bars represent one standard deviation. At 70 and 80°C,  $E_{R,CREV}$  was similar within experimental error in NaCl and CaCl<sub>2</sub> solutions for the two alloys. At 60°C,  $E_{R,CREV}$  values for alloys C-22 and HYBRID-BC1 in the CaCl<sub>2</sub> solution were 90-mV higher than in the NaCl solution. Figure 5 shows SEM images of alloy HYBRID-BC1 specimens tested in 4 mol/L NaCl and 2 mol/L CaCl<sub>2</sub> solutions, at 60°C. Abundant corrosion products were observed covering the attacked areas and around

them. The localized attack morphology of the tested alloys was the same at the three tested temperatures, in NaCl and CaCl<sub>2</sub> solutions.

Due to the discrepancies observed on the  $E_{R,CREV}$  values at 60°C, 24-hour constant potential tests were performed in 4 mol/L NaCl and 2 mol/L CaCl<sub>2</sub> solutions at -0.050 V<sub>SCE</sub> for alloy C-22, and at 0.150 V<sub>SCE</sub> for alloy HYBRID-BC1. The applied potentials are shown in Figure 4 (stars). Crevice corrosion initiated after similar incubation periods in both solutions for the two tested alloys. Crevice corrosion was not expected to occur in the 2 mol/L CaCl<sub>2</sub> solutions since the applied potential was lower than the previously determined  $E_{R,CREV}$ . Therefore, we concluded that the 4 mol/L NaCl and the 2 mol/L CaCl<sub>2</sub> solutions have the same aggressiveness regarding crevice corrosion. Apparent differences among  $E_{R,CREV}$  values determined in calcium and sodium chlorides may be attributed to an artifact from the PD-GS-PD technique when applied in CaCl<sub>2</sub> solutions, in certain conditions. Present results indicated that whenever possible,  $E_{R,CREV}$  values should be determined in NaCl solutions rather than in CaCl<sub>2</sub> solutions since they are more reliable and conservative.

**Corrosion potential in crevice-like solutions.**— This set of experiments in HCl solutions was performed to determine  $E_{CORR}^*$  which is a relevant parameter for the localized acidification model (Eq. 2). Further analyses of these results are out of the scope of the present paper.  $E_{CORR}^*$  is the minimum value that  $E_{R,CREV}$  can attain.<sup>21</sup>  $E_{CORR}$  varied less than 8 mV within the immersion time for all the tested temperatures.  $E_{CORR}$  stability of less than 1 mV/hour was obtained in most of cases after 30 minutes of immersion. The average value of  $E_{CORR}$  for each temperature was calculated from the last 10 minutes of immersion. The sampling rate was 0.5 Hz. Therefore,  $E_{CORR}$  was averaged among 300 values.

Electrolytes of 1 and 3 mol/L HCl were selected as candidate crevice-like solutions to determine  $E_{CORR}^*$  for each alloy. Considering the effect of chloride concentration in the proton activity, the pH values of the testing solutions were pH = 0 for 1 mol/L HCl and pH = -1 for 3 mol/L HCl.<sup>38,39</sup> The  $E_{CORR}$  of alloy 625 in 3 mol/L HCl was 40 mV higher than in 1 mol/L HCl and it was even higher than the  $E_{R,CREV}$  of alloy 625 in 5 mol/L CaCl<sub>2</sub> for temperatures above 70°C. Consequently, 3 mol/L HCl was considered too aggressive for alloy 625 and therefore a 1 mol/L HCl was selected as the crevice-like solution for this alloy. Alloys C-22, C-22HS and HYBRID-BC1 showed similar  $E_{CORR}$  values (within a 10-mV range) in 1 and 3 mol/L HCl for each temperature. This observation is in agreement with previous results indicating a very slight decrease of  $E_{CORR}$  for alloy C-22 in HCl solutions in the pH range from -1.75 to 0, at 90°C.<sup>39</sup> Taking into account the higher PRE of alloys C-22, C-22HS and HYBRID-BC1 compared to alloy 625, the crevice-like solution for these high PRE alloys was assumed to be 3 mol/L HCl, which is more aggressive than for alloy 625.

Figure 6 shows  $E_{CORR}$  of the tested alloys in the corresponding crevice-like solutions as a function of temperature.  $E_{CORR}$  showed a slight decrease from 30 to 70°C, then slightly increasing from 70 to 100°C for all the tested alloys. Alloy HYBRID-BC1 showed the lowest  $E_{CORR}$  variation in the studied temperature range. Alloys C-22 and C-22HS showed identical  $E_{CORR}$  values within experimental error in the studied conditions.  $E_{CORR}$  of alloys 625, C-22 and C-22HS decreased 30 to 40 mV when the temperature increased from 30 to 40°C. At higher temperatures,  $E_{CORR}$  remained in a 20-mV range.

Given the small spread of  $E_{CORR}$  of the tested alloys in the crevice-like solutions at temperatures above 40°C,  $E_{CORR}^*$  was assumed to be constant and equal to the average of the  $E_{CORR}$  values in the range from 40 to 100°C (Fig. 6). The obtained  $E_{CORR}^*$  values for each alloy are listed in Table II. In general,  $E_{CORR}^*$  increased with the PRE of the tested alloys.

**Effect of temperature.**— Figures 7–10 show  $E_{R,CREV}$  from PD-GS-PD tests on alloys 625, C-22, C-22HS and HYBRID-BC1, respectively, as a function of temperature (T) for the three tested chloride concentrations. Symbols are average values from at least three tests and the error bars represent one standard deviation. Equation 3 was

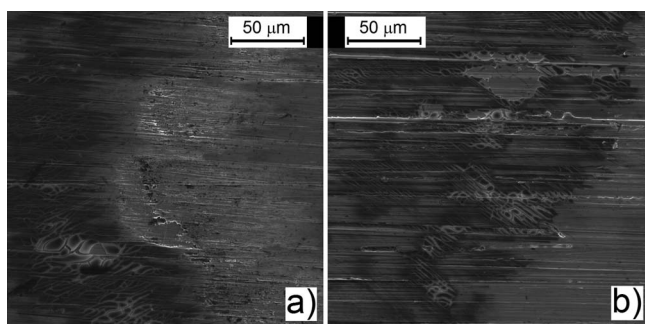


**Figure 5.** SEM images of alloy HYBRID-BC1 specimens after PD-GS-PD tests performed in a) 4 mol/L NaCl, and b) 2 mol/L CaCl<sub>2</sub>, at 60°C.

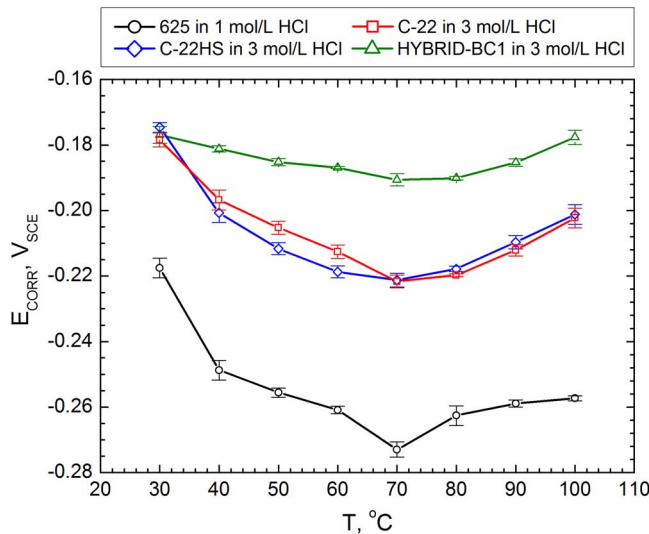


**Figure 6.**  $E_{\text{CORR}}$  of tested alloys as a function of temperature in HCl solutions simulating active crevices.

fitted to a range of the collected data for each alloy. Equation 3 is empirical and has been used by Dunn et al. for fitting to  $E_{\text{R,CREV}}$  data of alloy C-22 as a function of T and  $[\text{Cl}^-]$ .<sup>40</sup> A, B, C and D are constants which depend on each alloy. Figures 7–10 also show the fits of Equation 3 for the four Ni alloys. Comparison of the  $E_{\text{R,CREV}}$  values of the tested alloys as a function of T and  $[\text{Cl}^-]$  indicate that their corrosion resistance increased according to their corresponding PRE, being 625 < C-22 < C-22HS < HYBRID-BC1.

$$E_{\text{R,CREV}} = (A + BT)\log[\text{Cl}^-] + CT + D \quad [3]$$

Figure 7 shows that according to the model prediction, the obtained  $E_{\text{R,CREV}}$  values reached a limiting value for alloy 625 (the least corrosion resistant among tested alloys) above  $T^* = 90^\circ\text{C}$ .  $T^*$  was defined as the saturation temperature for  $E_{\text{R,CREV}}$ , i.e., the temperature at which  $E_{\text{R,CREV}}$  reaches its minimum limiting value. Consequently, Equation 3 was fitted to the obtained data only in the temperature range from 20 to  $90^\circ\text{C}$ . For alloys C-22 and C-22HS, the fitting of Equation 3 predicted that  $E_{\text{R,CREV}}$  reaches  $E_{\text{CORR}}^*$  near the highest testing temperatures:  $T^* = 110^\circ\text{C}$  for alloy C-22, and  $T^* = 120^\circ\text{C}$  for alloy C-22HS (Figs. 8 and 9, respectively). Equation 3 did not apply for  $T > T^*$  since in such conditions  $E_{\text{R,CREV}}$  was constant and equal to  $E_{\text{CORR}}^*$  (Figs. 7–9). For alloy HYBRID-BC1,  $E_{\text{R,CREV}}$  would reach  $E_{\text{CORR}}^*$  at  $T^* = 150^\circ\text{C}$ , which is well above the tested temperature range (Fig. 10). The highest testing temperatures were  $90^\circ\text{C}$  in the  $[\text{Cl}^-] = 0.1$  and 1 mol/L solutions and  $117^\circ\text{C}$  in the  $[\text{Cl}^-] = 10$  mol/L solution. The extrapolation of Equation 3 for dilute chloride solutions (0.1 and 1 mol/L) above  $90^\circ\text{C}$  are conservative estimations (Figs. 7–10). Table II shows the parameters obtained by least square fits of Equation 3 for the tested alloys along with the correlation coefficients ( $R^2$ ), the considered temperature ranges and the saturation temperatures. All the  $R^2$  values from the non-linear fits were above 0.9 which indicates that Equation 3 successfully represented  $E_{\text{R,CREV}}$  as a function of temperature and chloride concentration for the tested alloys. Statistically  $E_{\text{R,CREV}}$  may be considered to display a normal distribution around

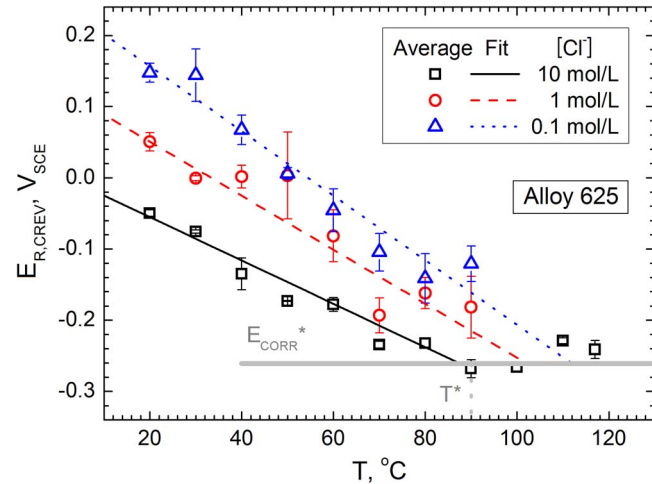


**Figure 7.**  $E_{\text{R,CREV}}$  of alloy 625 as a function of temperature. Average  $E_{\text{R,CREV}}$  values are represented along with the fit of Equation 3.

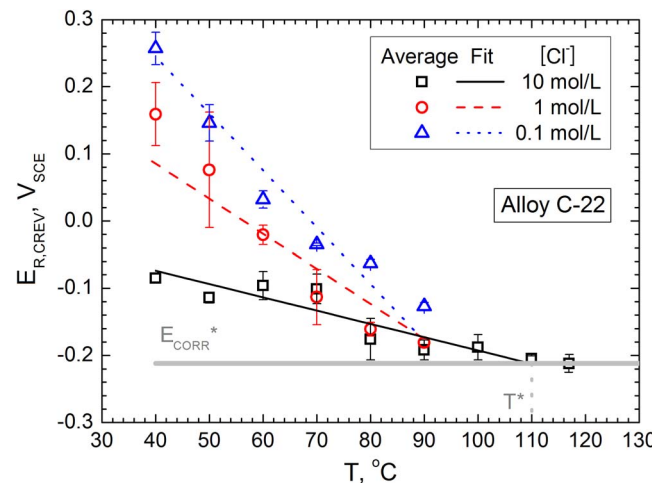


**Figure 8.**  $E_{\text{R,CREV}}$  of alloy C-22 as a function of temperature. Average  $E_{\text{R,CREV}}$  values are represented along with the fit of Equation 3.

the average values given by the fits (Table II). The parameter A indicates the variation of  $E_{\text{R,CREV}}$  with  $\log[\text{Cl}^-]$  independently of the temperature, while B indicates the temperature-dependent variation of  $E_{\text{R,CREV}}$  with  $\log[\text{Cl}^-]$ . Alloy 625 showed lower absolute values of A and B when compared to the other tested alloys indicating a slight dependence of  $E_{\text{R,CREV}}$  with  $\log[\text{Cl}^-]$  (Table II). Alloy C-22 and C-22HS showed the highest dependence of  $E_{\text{R,CREV}}$  with  $\log[\text{Cl}^-]$  among tested alloys. The parameter C states the temperature dependence of  $E_{\text{R,CREV}}$ , which was higher for alloys C-22 and C-22HS than for alloys 625 and HYBRID-BC1. The parameter D is an independent term which increased with the PRE of the alloys (Table II).

Figure 7 shows  $E_{\text{R,CREV}}$  of alloy 625 as a function of temperature for different chloride concentrations. Alloy 625 was tested in the temperature range from 20 to  $117^\circ\text{C}$ . The reported CCT for alloy

**Table II.** Corrosion potential of the alloys in the crevice-like solution and fit parameters of Equation 3 along with correlation coefficients, temperature ranges of fits and saturation temperature.

Alloy	$E_{\text{CORR}}^*, \text{V}_{\text{SCE}}$	A, $\text{V}_{\text{SCE}}$	B, $\text{V}/\text{K}$	C, $\text{V}/\text{K}$	D, $\text{V}_{\text{SCE}}$	$R^2$	T range	$T^*$
625	$-0.261 \pm 0.006$	$-0.121 \pm 0.015$	$0.00075 \pm 0.00025$	$-0.00379 \pm 0.00020$	$0.126 \pm 0.012$	0.901	20–90°C	90°C
C-22	$-0.212 \pm 0.008$	$-0.289 \pm 0.021$	$0.00324 \pm 0.00030$	$-0.00522 \pm 0.00027$	$0.294 \pm 0.019$	0.918	40–110°C	110°C
C-22HS	$-0.215 \pm 0.008$	$-0.267 \pm 0.024$	$0.00266 \pm 0.00032$	$-0.00494 \pm 0.00031$	$0.326 \pm 0.023$	0.916	40–117°C	120°C
HYBRID-BC1	$-0.184 \pm 0.005$	$-0.226 \pm 0.018$	$0.00176 \pm 0.00022$	$-0.00393 \pm 0.00020$	$0.363 \pm 0.016$	0.983	60–117°C	150°C

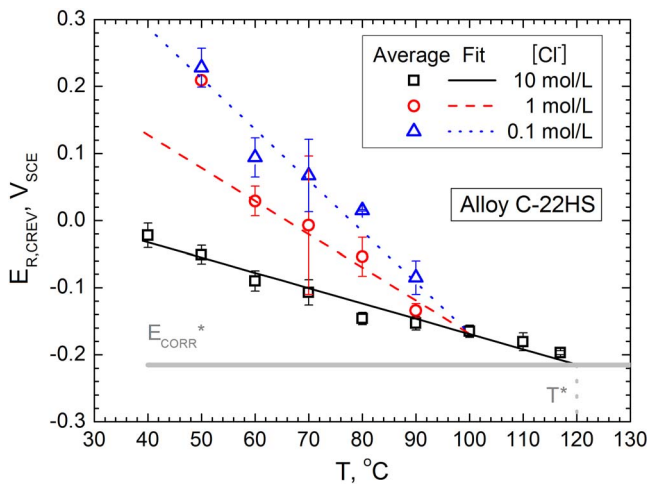


**Figure 9.**  $E_{R,CREV}$  of alloy C-22HS as a function of temperature. Average  $E_{R,CREV}$  values are represented along with the fit of Equation 3.

625 in the ASTM G 48 solution (immersion test Method D, acidified  $\text{FeCl}_3$ ) is  $40^\circ\text{C}$ .<sup>30</sup> However, current electrochemical results show that crevice corrosion occurred in the entire temperature range ( $20$  to  $117^\circ\text{C}$ ) in  $0.1$  to  $10$  mol/L chloride solutions. The CCT inferred from present results was lower than  $20^\circ\text{C}$ . Above  $100^\circ\text{C}$ , the measured  $E_{R,CREV}$  values for alloy 625 at  $[\text{Cl}^-] = 10$  mol/L showed a slight increase which might be due to an increase of  $E_{CORR^*}$ .

Figure 8 shows  $E_{R,CREV}$  of alloy C-22 as a function of temperature for different chloride concentrations. Alloy C-22 was tested in the temperature range from  $30$  to  $117^\circ\text{C}$ , showing crevice corrosion only at  $T \geq 40^\circ\text{C}$ , in all the tested solutions. The reported CCT for alloy C-22 in the ASTM G 48 solution is  $80^\circ\text{C}$ ,<sup>30</sup> while based on current results a CCT between  $30$  and  $40^\circ\text{C}$  was estimated.  $E_{R,CREV}$  showed a significant increase in the low temperature range for  $[\text{Cl}^-] = 0.1$  and  $1$  mol/L (Fig. 8). Present results for alloy C-22 were consistent with those of Mishra and Frankel<sup>17</sup> and those of Mishra and Shoesmith<sup>7</sup> but the current investigation found crevice corrosion at temperatures  $15$  to  $20^\circ\text{C}$  lower than previously reported.<sup>7,17</sup> Results of Dunn et al.<sup>40</sup> were dramatically less conservative since they used solid PTFE crevice formers (i.e. they did not use rigid ceramic washers). The crevice former materials significantly influence the measured  $E_{R,CREV}$  values being more relevant than the applied testing technique.<sup>5,10,11</sup>

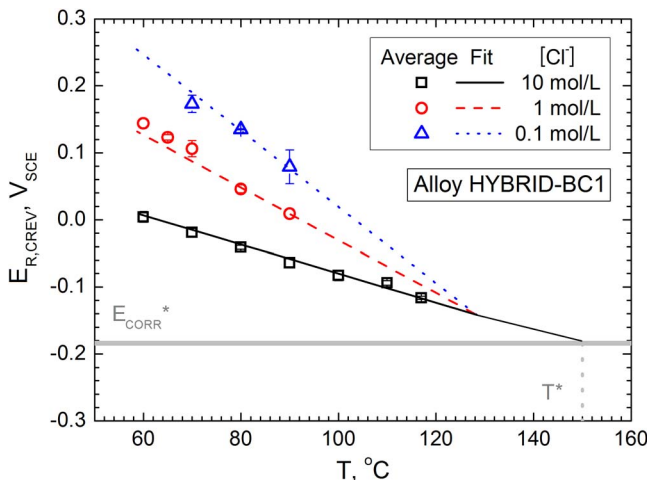


**Figure 10.**  $E_{R,CREV}$  of alloy HYBRID-BC1 as a function of temperature. Average  $E_{R,CREV}$  values are represented along with the fit of Equation 3.

Figure 9 shows  $E_{R,CREV}$  of alloy C-22HS as a function of temperature for different chloride concentrations. Alloy C-22HS was tested in the range from  $30$  to  $117^\circ\text{C}$ . Crevice corrosion was observed at  $T \geq 40^\circ\text{C}$  in  $[\text{Cl}^-] = 10$  mol/L solutions, and at  $T \geq 50^\circ\text{C}$  in  $[\text{Cl}^-] = 0.1$  and  $1$  mol/L solutions. The reported CCT for alloy C-22HS in the ASTM G 48 solution is  $100^\circ\text{C}$ .<sup>30</sup> From the present results, CCT was estimated between  $30$  and  $40^\circ\text{C}$ . Alloy C-22HS showed a  $E_{R,CREV}$  dependence with temperature and chloride concentration similar to that of alloy C-22. The fit parameters of the alloys C-22 and C-22HS were similar (Table II). Alloy C-22HS was slightly more crevice corrosion resistant than alloy C-22 in the tested conditions (which agrees well with the PRE values in Table I).

Figure 10 shows  $E_{R,CREV}$  of alloy HYBRID-BC1 as a function of temperature for different chloride concentrations. Alloy HYBRID-BC1 was tested in the range from  $50$  to  $117^\circ\text{C}$ . Crevice corrosion was observed at  $T \geq 60^\circ\text{C}$  in  $[\text{Cl}^-] = 1$  and  $10$  mol/L solutions, and at  $T \geq 70^\circ\text{C}$  in  $[\text{Cl}^-] = 0.1$  mol/L solutions. CCT for alloy HYBRID-BC1 in the ASTM G 48 solution is  $125^\circ\text{C}$ .<sup>30</sup> Present results indicated that CCT was between  $50$  and  $60^\circ\text{C}$ . Alloy HYBRID-BC1 was the most resistant to crevice corrosion among the tested alloys.

## Discussion

**Critical crevice temperature.**— The present results show that alloys 625, C-22 and C-22HS may suffer crevice corrosion below the CCT determined according to ASTM G 48.<sup>30</sup> This discrepancy is due to the higher aggressiveness of the PD-GS-PD tests compared to the standard immersion test in acidified  $\text{FeCl}_3$  solutions. The crevicing devices, i.e., the applied torque values, and materials (PTFE-wrapped ceramic), were more demanding in the present work than those used in ASTM G 48. Also, the crevicing washers in ASTM G 48 are made using solid PTFE materials which deform under pressure and do not form a tight firm crevice on the surface. Moreover, in the ASTM G 48 immersion test, there may be a limitation of the cathodic current that drives the anodic dissolution in the creviced spots since reduction reactions on the passive alloy may be inhibited. In the galvanostatic and potentiostatic electrochemical tests, the cathodic current has no limitations since the counter electrode supplies all the required current. The testing conditions used here may seem too aggressive for the alloys. However, it should be emphasized that present results would apply if a tight crevice is formed on the alloy surface and a cathodic reaction is available to support the anodic current demand inside the crevice. Under these conditions, the present results are not over conservative and may be applied to in-service conditions.

**Crevice corrosion dependence on environmental variables.**— The dependence of  $E_{R,CREV}$  with temperature and chloride concentration was studied for alloys 625, C-22, C-22HS and HYBRID-BC1. Equations 4 and 5 are the derivatives of  $E_{R,CREV}$  (Eq. 3) with respect to the logarithm of chloride concentration and with respect to temperature, respectively. Figure 11 shows  $-dE_{R,CREV}/d(\log[\text{Cl}^-])$  as a function of  $T$  (Eq. 4), and Figure 12 shows  $-dE_{R,CREV}/dT$  as a function of  $[\text{Cl}^-]$  (Eq. 5) for the tested alloys. The dashed lines in Figures 11 and 12 indicate the 95% confidence interval. As the environmental conditions became more aggressive (increase of  $T$  and  $[\text{Cl}^-]$ ) the absolute values of both slopes decreased indicating  $E_{R,CREV}$  was less dependent on the respective environmental variables.

$$-dE_{R,CREV}/d(\log[\text{Cl}^-]) = A + BT \quad [4]$$

$$-dE_{R,CREV}/dT = B \log[\text{Cl}^-] + C \quad [5]$$

Figure 11 shows the theoretical slope:  $-dE_{R,CREV}/d(\log[\text{Cl}^-]) = 2.3RT/F$ , where  $R$  is the universal gas constant and  $F$  is the Faraday constant. This slope is obtained by considering the ohmic potential drop between the alloy/solution interface within a pit/crevice and the bulk solution, as shown in Equation 6.<sup>21</sup>  $[\text{Cl}^-]_{\text{alloy/sol}}$  is the chloride concentration at the alloy/solution interface, which is generally almost saturated.<sup>22,26</sup> The chloride saturation concentration within crevices of

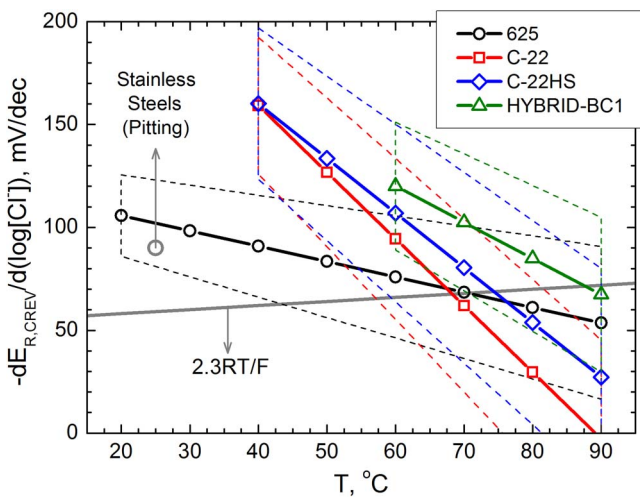


**Figure 11.** Derivative of  $E_{R,CREV}$  with respect to  $\log[Cl^-]$  as a function of the temperature.

Ni-Cr-Mo alloys is estimated to be 10 to 13 mol/L.<sup>26</sup> The absolute value of  $dE_{R,CREV}/d(\log[Cl^-])$  for the tested alloys decreased as temperature increased showing higher values than the theoretical slope in the low temperature range (Fig. 11). Laycock and Newman reported similar findings for pitting of stainless steels.<sup>22,24</sup> They attribute the high value of the slope to the formation of chloro-complexes of chromium<sup>22</sup> and the apparently anomalous temperature dependence of this slope to a gradual change in the dominant reaction path.<sup>24</sup> However, the theoretical slope only considers the ohmic potential drop in the solution, neglecting any additional contribution due to the ohmic drop in the corrosion products usually found covering the alloys.<sup>21</sup> The high experimental slopes found in the present study may be due to ohmic effects of passivating species at the alloy/solution interface, such as the polymeric molybdates found on alloy C-22.<sup>41</sup> The decrease of the values as temperature increased was attributed to the decrease of this additional ohmic drop.  $-dE_{R,CREV}/d(\log[Cl^-])$  approached the theoretical value ( $2.3RT/F$ ) above  $70^\circ C$  within the standard error, for all the tested alloys (Fig. 11).

$$\Delta\Phi = 2.3RT/F(\log[Cl^-]_{alloy/sol} - \log[Cl^-]) \quad [6]$$

Table III shows a literature review of  $-dE_{R,CREV}/d(\log[Cl^-])$  for alloy C-22 in hot chloride solutions. The slopes obtained by different testing methods using PTFE-wrapped ceramic crevice formers are in the range from 52 to 95 mV/dec.<sup>12,20,42</sup> In the present work, the slope for alloy C-22 was in the range from 0 to 50 mV/dec (Fig. 11). Differences among slopes may be ascribed to the tested chloride con-

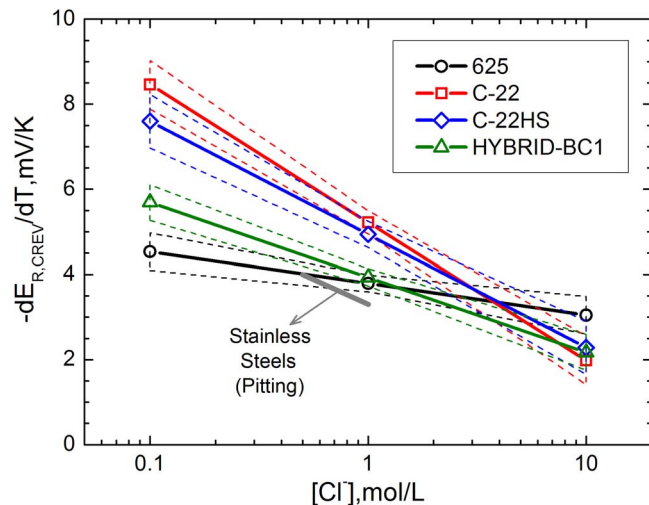


**Figure 12.** Derivative of  $E_{R,CREV}$  with respect to temperature as a function of the chloride concentration.

centration ranges. The slopes obtained by Dunn et al. using solid deformable PTFE crevice formers are higher than those from present results (from 75 to 360 mV/dec).<sup>40</sup> As explained above, the type of crevice formers materials play an important role in crevice corrosion testing.

Figure 12 shows the linear decrease of  $-dE_{R,CREV}/dT$  as a function of  $\log[Cl^-]$  for the tested alloys.  $E_{R,CREV}$  for alloys C-22 and C-22HS showed a higher temperature dependence than for alloys 625 and HYBRID-BC1 at  $[Cl^-] < 3$  mol/L. Alloys 625 and HYBRID-BC1 showed slopes similar to those of 300 series stainless steels for  $[Cl^-] = 0.5$  to 1 mol/L.<sup>24,32</sup> At  $[Cl^-] > 3$  mol/L, all the tested alloys showed similar temperature dependences with slopes from  $-3$  to  $-2$  mV/K. A slope of  $-6.2$  mV/K was estimated from Mishra and Frankel's data<sup>17</sup> for alloy C-22 in 1 mol/L NaCl, which is in agreement with the current results. Dunn et al.<sup>40</sup> reported slopes from  $-13.8$  to  $-11.5$  mV/K for MA alloy C-22. A comparison of current data and data from Dunn et al.<sup>40</sup> suggests that both slopes ( $-dE_{R,CREV}/d(\log[Cl^-])$ ) and  $-dE_{R,CREV}/dT$ ) may depend on the type of crevice former materials used.

*Crevice corrosion kinetics.*— The localized acidification model provides a mathematical expression for estimating  $E_{R,CREV}$  as a function of  $E_{CORR}^*$ ,  $\eta$  and  $\Delta\Phi$  (Eq. 2). In the present work, we obtained  $E_{R,CREV}$  from PD-GS-PD tests and measured  $E_{CORR}^*$  in crevice-like solutions. Then  $\eta$  and  $\Delta\Phi$  were calculated by a simplifying assumption as it is explained below.

**Table III.** Literature review of the slope  $-dE_{R,CREV}/d(\log[Cl^-])$  for alloy C-22 in different testing conditions.

Ref.	T, °C	Crevice formers	Testing technique*	Metallurgical condition**	[Cl^-], mol/L	$-dE_{R,CREV}/d(\log[Cl^-])$ , mV/decade	
40	80	Solid PTFE	PD-PS-PD	MA	0.5–5	180	
	125	torqued to 0.35 N.m		5'@870°C	0.01–5	75	
	60	PTFE-wrapped ceramic torqued to 5–8 N.m				360	
	95					230	
20	90	PTFE-wrapped ceramic torqued to 5–8 N.m	THE	MA	0.0005–1	86	
			CPP	MA & ASW	0.0005–4	95	
42		CPP	MA		0.0001–10	60	
			MA		0.1–4	52	
12		PD-GS-PD					

\*PD-PS-PD: Potentiodynamic-Potentiostatic-Potentiodynamic method; THE: Tsujikawa-Hisamatsu Electrochemical method; CPP: Cyclic Potentiodynamic Polarization method; PD-GS-PD: Potentiodynamic-Galvanostatic-Potentiodynamic method.

\*\*MA: Milled Annealed; 5'@870°C: thermally aged for 5 minutes at 870°C; ASW: As-welded.

$\Delta\Phi$  may be neglected in highly concentrated solutions. Equation 6 indicates that  $\Delta\Phi$  decreases as  $[Cl^-]$  increases and it becomes nil for  $[Cl^-] = [Cl^-]_{alloy/sol}$ . In the present case, a value of  $[Cl^-]_{alloy/sol} = 10$  mol/L was considered, which is near the reported saturation value for crevices of Ni-Cr-Mo alloys.<sup>26</sup> A similar assumption has been made before.<sup>6</sup> The absence of corrosion products in tests at  $[Cl^-] = 10$  mol/L (Fig. 2) suggests that there is no additional ohmic drop. Consequently, assuming  $\Delta\Phi = 0$  V for  $[Cl^-] = 10$  mol/L seems reasonable.

Equation 7 was obtained from Equations 2 and 3, evaluated at  $[Cl^-] = 10$  mol/L ( $\Delta\Phi = 0$  V) and it gives the value of  $\eta$  as a function of T. Since  $B + C < 0$  for all the tested alloys,  $\eta$  decreases linearly with the increase of temperature. In the present case,  $E_{CORR^*}$  was assumed to be constant between 40°C and 100°C due to its slight temperature dependence (Fig. 6). If  $E_{CORR^*}$  was a strong function on temperature,  $\eta$  would show a more complex temperature dependence. For instance,  $\eta$  for alloy 625 showed a non-linear temperature dependence below 40°C since  $E_{CORR^*}$  increased more than 30 mV (Fig. 6). The present analysis of crevice corrosion kinetics was restricted to temperatures of 40°C and above. Note that  $\eta$  and  $E_{CORR^*}$  are not functions of  $[Cl^-]$ .<sup>21</sup>

$$\eta = A + (B + C)T + D - E_{CORR^*} \quad [7]$$

Equation 8 gives the value of  $\Delta\Phi$  as a function of T and  $[Cl^-]$ . Equation 8 was obtained from Equations 2, 3 and 7 and it has the same form as Equation 6.  $\Delta\Phi$  decreases with the increase of T and  $[Cl^-]$ .  $\Delta\Phi$  is not affected by the assumption of a temperature-independent  $E_{CORR^*}$ .

$$\Delta\Phi = (A + BT)(\log[Cl^-] - 1) \quad [8]$$

Figure 13 shows a three-dimensional plot of  $E_{R,CREV}$  as a function of temperature and chloride concentration for alloy C-22.  $E_{CORR^*}$ ,  $\eta$  and  $\Delta\Phi$  were sequentially added to give  $E_{R,CREV}$  (Fig. 13).  $E_{CORR^*}$  does not depend on chloride concentration and it was considered to be constant with temperature in the tested conditions.  $\eta$  increased linearly below  $T^* = 110^\circ C$ , while it was nil above 110°C for alloy C-22.  $\Delta\Phi$  became an important contribution to  $E_{R,CREV}$  as  $[Cl^-]$  decreased below 90°C (Fig. 13).

Figure 14 shows  $\eta$  and  $\Delta\Phi$  in  $[Cl^-] = 1$  mol/L solutions as a function of temperature.  $\eta$  and  $\Delta\Phi$  decreased as temperature increased with slopes which depended on each alloy. In general,  $\eta$  increased as the PRE of the alloys increased. However, below 50°C, alloy 625 (PRE = 51) showed a slightly higher value for  $\eta$  than alloy C-22 (PRE = 70). Alloys C-22 and C-22HS showed a large  $\Delta\Phi$  at low temperatures but it became nil above 90 and 100°C, respectively. Alloys 625 and HYBRID-BC1 showed lower  $\Delta\Phi$  variations with temperature but a significant value of  $\Delta\Phi$  even above 100°C. However, unlike  $E_{CORR^*}$  and  $\eta$ ,  $\Delta\Phi$  did not increase with the PRE of the tested

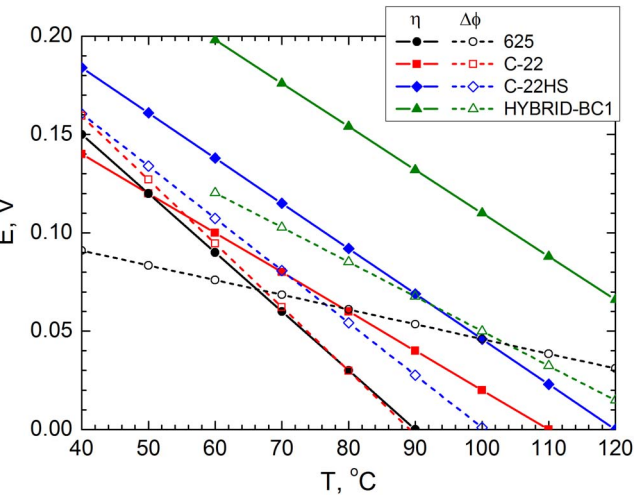


**Figure 14.** Anodic polarization to maintain crevice acidity ( $\eta$ ) and ohmic potential drop ( $\Delta\Phi$ ) in 1 mol/L chloride solutions as a function temperature for the tested alloys.

alloys. The trend of  $\Delta\Phi$  with the PRE depended on the temperature (Fig. 14). The present results suggest that PRE would be a good measure of the crevice corrosion resistance of the tested alloys only in concentrated chloride solutions where the contribution of  $\Delta\Phi$  is negligible. In dilute chloride solutions, the crevice corrosion resistance of the alloys might not have a direct correlation with PRE, since  $\Delta\Phi$  becomes the main contribution to  $E_{R,CREV}$ . This is in agreement with the findings of Sosa Haudet et al.<sup>43</sup> for a variety of nickel alloys in 0.1–10 mol/L chloride solutions, at 60°C. In  $[Cl^-] = 1$  mol/L solutions,  $\eta$  was higher than  $\Delta\Phi$  for alloys HYBRID-BC1 and C-22HS in the entire temperature range (Fig. 14). For alloy C-22,  $\eta$  was higher than  $\Delta\Phi$  only above 56°C. For alloy 625, a completely different behavior was observed since  $\eta$  was higher than  $\Delta\Phi$  below 66°C, while  $\Delta\Phi$  became the main contribution to  $E_{R,CREV}$  above 66°C (Fig. 14). This finding suggests that as the crevice corrosion resistance of the alloys increases  $\eta$  becomes a more important contribution to  $E_{R,CREV}$  when compared to  $\Delta\Phi$ .

The application of the localized acidification model allowed a better understanding of the relative contributions of  $E_{CORR^*}$ ,  $\Delta\Phi$  and  $\eta$  to  $E_{R,CREV}$  at different temperatures for the tested alloys.  $E_{CORR^*}$  alone explained neither the different crevice corrosion resistances of the alloys (it was in a 80-mV range for the tested alloys) nor the temperature dependence of  $E_{R,CREV}$ . The relative contributions of  $\Delta\Phi$  and  $\eta$  and their dependence with temperature explains the observed behavior of  $E_{R,CREV}$ .

## Conclusions

The crevice corrosion resistance of alloys 625, C-22, C22HS and HYBRID-BC1 was assessed in 0.1 to 10 mol/L chloride solutions at temperatures ranging from 20°C to 117°C. Alloy 625 suffered crevice corrosion in the entire temperature range, alloys C-22 and C-22HS suffered crevice corrosion at 40°C and higher temperatures, while alloy HYBRID-BC1 suffered crevice corrosion at 60°C and higher temperatures. The results show that the studied Ni alloys may suffer crevice corrosion tens of degrees below the reported critical crevice temperatures obtained through immersion tests.

Comparison of the crevice corrosion behavior of alloys C-22 and HYBRID-BC1 in 4 mol/L NaCl and 2 mol/L CaCl<sub>2</sub> solutions indicated that both solutions have the same aggressiveness regarding crevice corrosion. However, crevice corrosion repassivation potential values should be determined in NaCl solutions rather than in CaCl<sub>2</sub> solutions whenever possible, since the former are more reproducible and conservative. The explanation of this behavior needs further research.

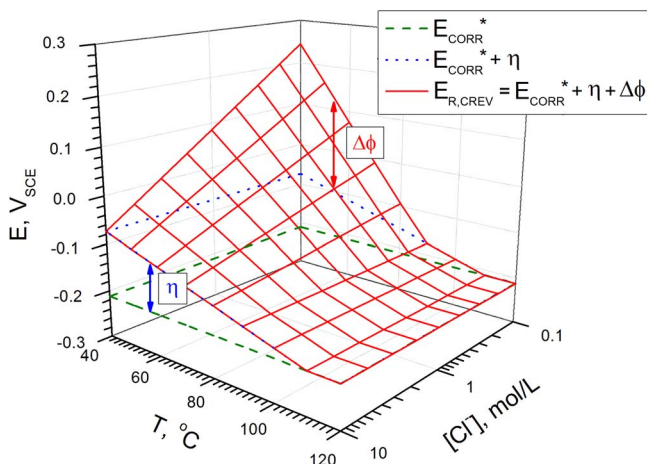


**Figure 13.**  $E_{CORR^*}$ ,  $E_{CORR^*} + \eta$  and  $E_{R,CREV}$  for alloy C-22 as a function of temperature and chloride concentration.

The repassivation potential of the tested alloys as a function of temperature and chloride concentration is given by  $E_{R,CREV} = (A + BT)\log[Cl^-] + CT + D$  for a range of environmental conditions. When the temperature and chloride concentration increased  $E_{R,CREV}$  showed a lesser dependence on the environmental variables. For alloys 625 and C-22,  $E_{R,CREV}$  reached a minimum limiting value which was coincident with the corrosion potential in the crevice-like solution. For alloys C-22HS and HYBRID-BC1,  $E_{R,CREV}$  is expected to reach its minimum limiting value above 120°C and 150°C, respectively.

The slope  $-dE_{R,CREV}/d(\log[Cl^-])$  was higher than the theoretical value ( $2.3RT/F$ ) which was attributed to additional ohmic effects of passivating species at the alloy/solution interface. The decrease of  $-dE_{R,CREV}/d(\log[Cl^-])$  as temperature increased was linked to the decrease of this additional ohmic drop.  $E_{R,CREV}$  for alloys C-22 and C-22HS showed a higher temperature dependence than for alloys 625 and HYBRID-BC1 at  $[Cl^-] < 3 \text{ mol/L}$ . At  $[Cl^-] > 3 \text{ mol/L}$ , all the tested alloys showed similar temperature dependences with a slope from  $-3$  to  $-2 \text{ mV/K}$ .

According to the localized acidification model,  $E_{R,CREV}$  is the sum of three contributions:  $E_{CORR}^*$ ,  $\eta$  and  $\Delta\Phi$ .  $E_{CORR}^*$  was insensitive to temperature changes while  $\eta$  and  $\Delta\Phi$  decreased linearly as the temperature decreased with slopes which depended on each alloy.  $E_{CORR}^*$  and  $\eta$  increased with the PRE, while the dependence of  $\Delta\Phi$  with PRE was a function of the temperature. Consequently, the PRE may be a good measure of the crevice corrosion resistance of nickel alloys containing chromium and molybdenum only in concentrated chloride solutions, while in dilute chloride solutions the crevice corrosion resistance might not be a direct function of PRE.

### Acknowledgments

Financial support from the Agencia Nacional de Promoción Científica y Tecnológica of the Ministerio de Educación, Ciencia y Tecnología from Argentina, and from the Universidad Nacional de San Martín is acknowledged.

### References

- D. C. Agarwal and N. Sridhar, in *Uhlig's Corrosion Handbook*, p. 837, John Wiley & Sons, Inc. (2011).
- Z. Szklarska-Smialowska, *Pitting and Crevice Corrosion*, NACE International, Houston, TX, USA (2005).
- R. B. Rebak, in *Material Science and Engineering. A Comprehensive Treatment*, R. W. Cahn, P. Haasen, and E. J. Kramer, Editors, p. 69, Wiley-VCH, Weinheim, Germany (2000).
- J. R. Galvele, *Corrosion Science*, **47**, 3053 (2005).
- M. A. Rodríguez, R. M. Carranza, and R. B. Rebak, *Corrosion*, **66**, 015007 (2010).
- N. S. Zadorozne, C. M. Giordano, M. A. Rodríguez, R. M. Carranza, and R. B. Rebak, *Electrochimica Acta*, **76**, 94 (2012).
- A. K. Mishra and D. W. Shoesmith, *Corrosion*, **70**, 721 (2014).
- R. B. Rebak, in *Corrosion 2005*, Paper N° 05610, NACE International, Houston, TX, USA (2005).
- R. M. Carranza, *JOM Journal of the Minerals, Metals and Materials*, **60**, 58 (2008).
- C. M. Giordano, M. Rincón Ortíz, M. A. Rodríguez, R. M. Carranza, and R. B. Rebak, *Corrosion Engineering Science and Technology*, **46**, 129 (2011).
- X. Shan and J. H. Payer, *Corrosion*, **66**, 105005 (2010).
- M. Rincón Ortíz, M. A. Rodríguez, R. M. Carranza, and R. B. Rebak, *Corrosion*, **66**, 105002 (2010).
- X. He, D. S. Dunn, and A. A. Csontos, *Electrochimica Acta*, **52**, 7556 (2007).
- P. Jakupi, J. J. Noel, and D. W. Shoesmith, *Corrosion Science*, **53**, 3122 (2011).
- M. A. Rodríguez, R. M. Carranza, and R. B. Rebak, in *Corrosion 2009*, Paper N° 09424, NACE International, Houston, TX, USA (2009).
- M. Rincón Ortíz, M. A. Rodríguez, R. M. Carranza, and R. B. Rebak, *Corrosion Science*, **68**, 72 (2013).
- A. K. Mishra and G. S. Frankel, *Corrosion*, **64**, 836 (2008).
- B. A. Kehler, G. O. Ilevbare, and J. R. Scully, *Corrosion*, **57**, 1042 (2001).
- B. A. Kehler and J. R. Scully, *Corrosion*, **61**, 665 (2005).
- K. J. Evans, A. Yilmaz, S. D. Day, L. L. Wong, J. C. Estill, and R. B. Rebak, *JOM Journal of the Minerals, Metals and Materials*, **57**, 56 (2005).
- J. R. Galvele, *Journal of The Electrochemical Society*, **123**, 464 (1976).
- R. C. Newman, *Corrosion*, **57**, 1030 (2001).
- N. J. Laycock, J. Stewart, and R. C. Newman, *Corrosion Science*, **39**, 1791 (1997).
- N. J. Laycock and R. C. Newman, *Corrosion Science*, **40**, 887 (1998).
- R. C. Newman, M. A. A. Ajjawi, H. Ezuber, and S. Turgoose, *Corrosion Science*, **28**, 471 (1988).
- F. Bocher, R. Huang, and J. R. Scully, *Corrosion*, **66**, 055002 (2010).
- P. T. Jakobsen and E. Maahn, *Corrosion Science*, **43**, 1693 (2001).
- S. Valen and P. O. Gartland, *Corrosion*, **51**, 750 (1995).
- E. A. Abd El Meguid and A. A. Abd El Latif, *Corrosion Science*, **46**, 2431 (2004).
- G. O. Ilevbare, *Corrosion*, **62**, 340 (2006).
- M. Ürgen and A. F. Çakir, *Corrosion Science*, **32**, 835 (1991).
- H-2122 HASTELLOY C-22HS alloy preliminary data, Haynes International (2005); H-3179a HASTELLOY HYBRID-BC1 alloy, Haynes International (2014).
- Standard Test Method for Determining the Crevice Repassivation Potential of Corrosion-Resistant Alloys Using a Potentiodynamic-Galvanostatic-Potentiostatic Technique, ASTM G192, in *Annual Book of ASTM Standards*, ASTM International, West Conshohocken, PA (2008).
- E. Rodil and J. H. Vera, *Fluid Phase Equilibria*, **187–188**, 15 (2001).
- R. G. Bates, B. R. Staples, and R. A. Robinson, *Analytical Chemistry*, **42**, 867 (1970).
- P. Jakupi, J. J. Noel, and D. W. Shoesmith, *Electrochemical and Solid-State Letters*, **13**, C1 (2010).
- R. M. Carranza and R. B. Rebak, in *MRS Symposium Proceedings Vol. 1193, Scientific Basis for Nuclear Waste Management XXXIII*, B. E. Burakov and A. S. Aloy, Editors, p. 569, Cambridge University Press, New York, NY, USA (2009).
- R. S. Lillard, M. P. Jurinski, and J. R. Scully, *Corrosion*, **50**, 251 (1994).
- M. A. Rodríguez, R. M. Carranza, and R. B. Rebak, *Journal of The Electrochemical Society*, **157**, C1 (2010).
- D. S. Dunn, Y.-M. Pan, L. Yang, and G. A. Cagnolino, *Corrosion*, **62**, 3 (2006).
- P. Jakupi, F. Wang, J. J. Noel, and D. W. Shoesmith, *Corrosion Science*, **53**, 1670 (2011).
- R. M. Carranza, M. A. Rodríguez, and R. B. Rebak, *Corrosion*, **63**, 480 (2007).
- S. Sosa Haudet, M. A. Rodríguez, and R. M. Carranza, in *MRS Symposium Proceedings Vol. 1475, Scientific Basis for Nuclear Waste Management XXXV*, R. M. Carranza, G. S. Duffó, and R. B. Rebak, Editors, p. 489, Cambridge University Press, New York, NY, USA (2012).